Frequency- and Time- Domain Dependency of Electrical Properties of Cement-Based Materials During Early Hydration

Frequency- and Time- Domain Dependency of Electrical Properties of Cement-Based Materials During Early Hydration

Hussameldin M. Taha[1]

William J. McCarter[1] *

Benny Suryanto[1]

Gerry Starrs[1]

[1]Heriot Watt University, School of Energy, Geoscience, Infrastructure and Society, Institute for Infrastructure and Environment, Edinburgh, EH14 4AS, U.K.

* Corresponding Author
E-mail: w.j.mccarter@hw.ac.uk
Tel: +44 (0)131 451 3318
Fax: +44 (0)131 451 4617

Abstract:

The electrical properties of Portland cement, and cements containing supplementary cementitious materials (SCM), were obtained over the frequency range 1kHz-10MHz during the initial 24-hours after gauging with water. The response was measured in terms of conductivity and permittivity with both parameters exhibiting significant temporal changes during this period. It was also evident that whilst the conductivity increased only marginally with increasing frequency of applied electrical field, the permittivity decreased by several orders of magnitude over this frequency range. Moreover, certain features of the permittivity response – which are related to bulk polarization processes – only revealed themselves in the higher frequency range (100kHz-1MHz), and went undetected at lower frequencies. The detailed frequency- and time- domain measurements allowed identification of several stages in the early hydration of cement-based materials and the response can be interpreted in terms of hydration kinetics, physico-chemical processes and microstructural development. It is shown that the methodology can be equally applied to cement-pastes and concretes.

Keywords: Cement, hydration, kinetics, electrical properties, conductivity, permittivity, supplementary cementitious materials.

Introduction

Cement hydration, including hydrolysis, poly-condensation and crystallization, is associated with heat changes and the exothermal nature of the reaction is widely used to monitor the early-age (<24-hours) processes. However, the development of the microstructure is not readily identifiable from the heat-flux profiles measured by conduction calorimetry and additional tests such as scanning electron microscopy (SEM), environmental SEM, back-scatter electron (BSE) imaging and X-ray diffraction can be used to provide supporting information on microstructural development. There is a need to develop a viable, complementary testing methodology capable of continuously monitoring the setting and hardening processes under non-isothermal conditions, as is the case in normal concreting operations, and simultaneously providing information on microstructural development and physico-chemical processes.

The use of electrical property measurements to study cement hydration is a developing field and such measurements have not been fully exploited in characterizing the hydration process although some early work was encouraging in this respect [1-3]. The intrinsic electrical properties of any non-magnetic material can be fully specified by the frequency dependent parameters relative permittivity, $\varepsilon_r(\omega)$, and conductivity, $\sigma(\omega)$, which are dependent upon the polarization and conduction of bound and free charges within the material. If the material is heterogeneous, $\varepsilon_r(\omega)$ and $\sigma(\omega)$ will be strongly correlated to the properties of the individual components and the way in which they are combined. It is, therefore, possible to identify and characterize porous cementitious materials by their electrical properties provided these are observed over a wide enough frequency range. A considerable amount of work has been presented on the electrical properties of cementitious materials to study the hardening process (i.e. periods > 24-hours). In a similar fashion, the electrical conductivity (and its reciprocal,

resistivity) of cement pastes has been used to study the initial 24-hours of the hydration process [see, for example, 4-16], although studies on the relative permittivity over the same period are much more limited [see, for example, 17-21]. An important aspect, and limitation, of early-age measurements to date being that these are generally obtained at a fixed frequency of applied electrical field or over a very limited frequency range. Regarding the latter, conductivity measurements tend to be taken in the low kilohertz range (100Hz-10kHz) whereas relative permittivity measurements are generally measured in the gigahertz (GHz) region.

The conductivity of hydrating cement-paste is related to both the conductivity of the pore fluid (hence ionic concentration within the pore fluid) and the continuity and tortuosity of the pore network. The relative permittivity, on the other hand, is associated with polarization processes operative within the paste that are, themselves, related to the mobility of charges adsorbed on the grain and crystal surfaces and at crystal/pore-water interfaces. It is set against this background that this paper presents a detailed electrical spectroscopy study on the early hydration of cementitious materials to study hydration kinetics and physico-chemical processes. Complex impedance data - from which conductivity, $\sigma(\omega)$, and relative permittivity, $\varepsilon_r(\omega)$, are subsequently derived - are acquired over the frequency range 1kHz-10MHz during the initial 24-hours after gauging with water. It is shown that a multi-frequency approach to electrical property measurements can reveal more information than single-frequency measurements.

Experimental Program

MATERIALS AND SAMPLE PREPARATION

In the current work, the binders comprised a Portland cement (PC) clinker, CEM I 52.5N to EN197-1 [22] and CEM I (ASTM Type I) cement blended with ground granulated blast-furnace slag (GGBS) to EN15167-1 [23] at 35%, 50% and 65% replacements levels. A typical oxide composition of the materials is presented in Table 1. The water-binder (w/b) ratios for the plain CEM I paste samples were 0.30, 0.35 and 0.45; the pastes containing GGBS had a fixed w/b ratio of 0.35. The mix proportions for the concretes used in the experimental program are presented in Table 2 and comprised a plain CEM I cement concrete (PCC) and two concretes with 35% and 65% replacement levels of GGBS. A w/b ratio of 0.45 was used to ensure workability without the need for the addition of plasticiser.

The paste samples were compacted into perspex cuboidal cells of internal dimensions 50mm×50mm×50mm whereas the cells for the concrete samples were 150mm×150mm×150mm. A pair of stainless steel electrodes, 2.4mm diameter with a center-to-center spacing of 25mm were embedded centrally inside the paste samples to a depth of 25mm; for the concrete samples, the center-to-center spacing was 75mm embedded to a depth of 75mm. Embedding the electrodes in this fashion ensured intimate contact with the sample and reduced any interference with the natural distribution of aggregate in the case of concretes. In addition, the internal temperature of the samples was measured by embedding a thermistor within each sample at the time of casting. The top surface of the cell was covered to prevent evaporation with tests carried out in a temperature controlled laboratory (22°C±1°C).

ELECTRICAL MEASUREMENTS AND DATA PROCESSING

A Solartron 1260 frequency response analyzer (FRA) was used to perform a logarithmic measurement sweep in the frequency range 1kHz-10MHz using 10 frequency points per decade. Screened BNC coaxial leads were used to connect to the FRA whereas at the sample end, connection to the electrodes was by means of alligator clips. The impedance of the sample (see Eq (1) below) was taken at each test frequency. Due to the low electrical impedance of the samples during the early stages, lead inductive and stray capacitance can degrade measurements as the frequency of the electrical field increases. In this work these effects were *nulled* from the measurements at each test frequency by utilizing a measurement conversion protocol implemented in Microsoft Excel that is based on two sets of calibration data that had been acquired prior to the start of testing, which comprised,

(i) An open-circuit sweep: electrical measurements with air between the electrodes in the test cell;

(ii) A short-circuit sweep: electrical measurements with the electrodes connected by a small stainless steel shorting bar;

From this sequence of measurements the true sample impedance, $Z(\omega)$, at each test frequency was obtained from the measured data. It should be noted that due to the low impedances being measured, even using this nulling protocol results in excess of approximately 5MHz showed increased scatter and for that reason only data up to 1MHz are presented. Measurement sweeps were initiated on a 4 minute cycle throughout the initial 24-hours after gauging.

The impedance, $Z(\omega)$, of the sample, obtained as above, can be written as,

$$Z(\omega) = Z'(\omega) - iZ''(\omega) \quad (1)$$

where $Z'(\omega)$ is the in-phase or resistive component and $Z''(\omega)$ is the quadrature or reactive component. At any angular frequency, ω, the electrical response of such a system will result from the superposed phenomena of conduction and polarization (discussed below). These are quantified, respectively, by the bulk conductivity, σ(ω), and relative permittivity, $\varepsilon_r(\omega)$, which are obtained from the impedance through the following relationships,

$$\sigma(\omega) = \left(\frac{Z'(\omega)}{Z'(\omega)^2 + Z''(\omega)^2}\right)\frac{L}{A} \tag{2}$$

$$\varepsilon_r(\omega) = \frac{1}{\varepsilon_o \omega}\left(\frac{Z''(\omega)}{Z'(\omega)^2 + Z''(\omega)^2}\right)\frac{L}{A} \tag{3}$$

where ε_o is the permittivity of a vacuum (8.854×10^{-12} Farads/m); L/A is a factor which is related to the electrode geometry and sample configuration. As the electrical field between the electrodes is non-uniform, the geometrical factor L/A in equations (2) and (3) cannot be readily calculated and was evaluated by calibrating the electrode array using a liquid of known electrical properties. For the electrode arrangements used in the current work, the geometrical factor L/A was evaluated as 41.67 m^{-1} for the paste electrode arrangement, and 17.34m^{-1} for the concrete electrode arrangement. Regarding the relative permittivity, it was found that this can change by more than four orders of magnitude over the frequency range 1kHz-10MHz. In order to present the responses on a single figure, the *normalised* permittivity, $\varepsilon_N(\omega)$ at frequency ω, was used and is defined this as the ratio of the relative permittivity at time, t, after the start of the test, $\varepsilon_{r,t}(\omega)$, to the relative permittivity at the start of the test, $\varepsilon_{r,o}(\omega)$ (i.e. time, t = 0), hence,

$$\varepsilon_N(\omega) = \frac{\varepsilon_{r,t}(\omega)}{\varepsilon_{r,o}(\omega)} \tag{4}$$

Results and Discussion

PRELIMINARIES

The response of the cementitious system to an alternating electrical field will be directly related to both conduction and polarization processes operative within the material. The permittivity, $\varepsilon_r(\omega)$, is a measure of the polarizability of the system and, at a particular frequency of applied field, quantifies the sum total of all polarization processes operative at that frequency. Polarization can be described as the displacement of opposite charges in parallel with an applied electric field from their zero-field equilibrium position. Several mechanisms contribute to polarization and each mechanism has a characteristic relaxation frequency. As the frequency increases, the slower (i.e. low-frequency) polarization mechanisms are unable to follow the alternations of the applied electrical field and therefore unable to contribute to the permittivity. This results in a decrease in permittivity with increasing frequency (i.e. relaxation). With reference to Fig. 1, typical polarization processes include:

(i) Double-layer polarization (Fig. 1a) which arises from the displacement of the double-layer counterion cloud relative to the charged particle in response to the applied electric field. This can induce large dipoles which will give rise to a high capacitance, hence permittivity. Double-layer polarisation is a low frequency mechanism [24, 25].

(ii) Interfacial or space charge polarization (Fig. 1b) occurring in heterogeneous systems when more than one material component is present and when translating charge carriers become *trapped* or *blocked* at the interfaces within the material. This results in an accumulation of charges thereby increasing the overall capacitance of the system. This is an intermediate frequency mechanism (high kHz-MHz) [26].

Conductivity can be regarded as a measure of all loss processes operative within the material and quantifies the energy dissipated by the motion of free charges in an applied electric field. Within the dynamic range under consideration, this would be dominated by the movement of ions in the continuous, water-filled capillary pore network (i.e. ionic conduction process), however, losses associated with relaxation/dispersion of the polarization process (i.e. double-layer and interfacial) will also contribute to the conductivity. The cumulative effect of these losses would result in an increase in conductivity with increasing frequency, hence the conductivity, $\sigma(\omega)$, can be written more completely as,

$$\sigma(\omega) = \sigma_d(\omega) + \sigma(0) \quad (5)$$

where $\sigma(0)$ is the low-frequency (ionic) conductivity and $\sigma_d(\omega)$ quantifies the losses resulting from dissipative polarization processes.

Conduction and polarization processes will thus be intimately related to pore-fluid chemistry, surface reactivity, hydration and the continuously evolving microstructure and, as a consequence, they will not only frequency-dependent but also time-variant. It should also be noted that in addition to the bulk polarization phenomena detailed in Fig. 1, electrode polarization also manifests itself in the low-frequency range. This is a well know phenomenon which takes place at the interface between a metallic electrode and an ionically conducting material and is due to the accumulation of a spatial charge on the surface of electrodes. Electrode polarization effects are generally avoided by using a sufficiently high frequency of applied electric field.

GENERAL OBSERVATIONS AND SALIENT FEATURES

Note that in the Figures discussed below, for reasons of clarity only every 10^{th} measurement point is highlighted on the Figures.

(a) CEM I Mixes

Fig. 2a presents the conductivity, σ, for the Portland cement pastes at the three water/binder ratios during the initial 24-hours after gauging, with measurements presented at a frequency of 100kHz - this frequency being a priori optimized to ensure electrode polarization had a negligible effect on measurements and the bulk response was obtained. Fig. 2b presents an enlargement of the response over the initial two and a half hours. Considering Figs. 2a and 2b, similar features are clearly evident on all three curves although the time at which they occur and their prominence are related to the w/b ratio. In general terms, the curves can be divided into two distinct regions: a period of increasing conductivity reaching a maximum within 1.0-1.5 hours followed by a period of decreasing conductivity over the remainder of the test period. For comparative purposes, Fig. 2c displays the change in temperature within the pastes, with the increase in temperature resulting from the setting process. Fig. 2c is not dissimilar to the rate of heat output from conduction calorimetry studies, although the work presented here was carried out under conditions which were more semi-adiabatic than isothermal (and, therefore, more representative of practice).

By considering the rate of change of the conductivity [27] over the test-period, these two regions can be further subdivided. Fig. 3a presents the derivative, $d\sigma/dt$, of the curves presented in Fig. 2a over the initial 15 hours. For illustrative purposes, Fig. 3b presents both the conductivity and its derivative ($d\sigma/dt$) versus time curves for the w/b = 0.35 paste. Due to the short time interval between measurements, considerably more detail can be detected than

has hitherto been obtained such that within the 24-hour test period, six regions in the conductivity response, and its derivative, can now be delineated and denoted I-VI:

Region I: an initial period of rapidly increasing conductance which reduces markedly after approximately 30 minutes.

Region II: is characterised by a period of slowly increasing conductance and continually reducing $d\sigma/dt$, which culminates in a global maximum in conductivity at approximately 1.5 hours after gauging, although its time of occurrence depends on the w/b ratio - increasing with increasing w/b ratio. The conductivity maximum signifies the start of the continual decrease in conductivity (i.e. negative $d\sigma/dt$ values);

Region III: this is a short-lived region of rapidly decreasing conductivity occurring over the period 1.5-2.0 hours and results in a local minimum on the $d\sigma/dt$ curve;

Region IV: the period 2.0-6.5 hours represents a region of decreasing conductivity; $d\sigma/dt$ values reduce (i.e. become more negative) over the period 2.0-4.0, attaining an almost constant value over the remained of this period;

Region V: this region (6.5-9.5 hours) is identified as a region over which a *shoulder* or *saddle* develops in the conductivity curve which manifests itself as a local maximum on the $d\sigma/dt$ curve; and,

Region VI: this region (>9.5 hours) occurs at the point where the $d\sigma/dt$ curve starts to increase (i.e. gradient becomes less negative) with time with the conductivity gradually reducing over the remainder of the test period.

Fig. 4 presents the change in normalised permittivity, $\varepsilon_N(\omega)$, over the 24-hour test period for the three w/b ratios; Fig. 4b also indicates the times over which the six regions occur as identified from the conductivity response in Fig. 3b for the w/b=0.35 paste. Although

measurements were recorded at 40 frequencies at every time-step, for clarity, ε_N is presented at five spot frequencies extending over three orders of magnitude: 1kHz, 100kHz, 200kHz, 500kHz and 1MHz. It should be noted that although the relative change in permittivity is presented for each w/b ratio on Fig. 4, the absolute values of permittivity decrease by almost three orders of magnitude as the frequency increases from 1kHz to 100kHz and by a factor of approximately 25 as the frequency increases from 100kHz to 1MHz. Table 3 presents initial permittivity values ($\varepsilon_{r,o}(\omega)$) for the plain cement pastes.

Fig. 4 clearly highlights the effect of the applied frequency on the response – at low-frequencies (i.e. 1kHz), the permittivity response virtually mimics the change in conductivity presented in Fig. 2a; however, as the frequency increases, several features are revealed which become more defined with increasing frequency and to highlight these, Fig. 5a presents the ε_N value for the cement pastes at 1MHz. From this Figure, a number of *peaks* (or local maxima) can be detected with each peak signifying an increase in polarizability of the paste. The first peak (denoted P_1 on this Figure) is only detected in the paste with w/b = 0.45 and coincides with the time at which the maximum value in conductivity occurs; for comparison, the time at which the conductivity maximizes for the w/b = 0.30 and 0.35 pastes is indicated on the respective permittivity curve. All responses display a peak (denoted P_2) which develops within the time period 2.5-6.0 hours for w/b = 0.30; 3.5-7.0 hours for w/b = 0.35, and 4.0-7.0 hours for w/b = 0.45. An additional peak (denoted P_3) occurs at approximately 9.0 hours for w/b = 0.30; 10.5 hours for w/b = 0.35, 14.5 hours for w/b = 0.45, although P_3 is only weakly developed for the w/b = 0.30 and 0.35 pastes. Fig. 5b presents an enlargement of the w/b = 0.35 paste at 1MHz which is further discussed below.

(b) GGBS Mixes

Fig. 6 presents the conductivity (Fig. 6a) and its derivative (Fig. 6b) for the pastes with slag replacement levels of 35%, 50% and 65% (w/b = 0.35) during the initial 24-hours. This Figure is similar to Figs. 2a and 3a in terms of the overall profile and features, although the absolute values of the conductivity and dσ/dt are much reduced. It is apparent that the addition of slag reduces the value of the early conductivity peak - the pure Portland cement mix recorded a maximum value of 1.70S/m (w/b = 0.35) whereas replacement levels of 35%, 50% and 65% GGBS obtained maximum values of 1.16S/m, 1.11S/m and 0.87S/m respectively, which indicates an inverse relationship between conductivity and the slag replacement level during the early stages of hydration, whereas at times in excess of ~13 hours this relationship reverses. This indicates a reduction in ionic concentration within the interstitial aqueous phase during the early stages and an overall reduction in hydration process and reaction kinetics with increasing level of replacement at the latter stages of the 24-hour test period.

Again, for illustrative purposes, Fig. 6c presents both the conductivity, and its derivative, for 50% GGBS replacement over the initial 15-hours with the six regions, discussed above in relation to plain cement paste, are indicated on this Figure. Comparing the GGBS mix with the plain cement-paste in Fig. 3b, it is evident that the addition of GGBS causes an increase in the duration of region III and, from the dσ/dt curve, a broader maximum occurring within region V. Fig. 6d presents the change in internal temperature of the GGBS samples.

Fig. 7 presents the change in the normalised permittivity over the initial 24-hours for the three GGBS replacement levels at the indicated frequencies. Peak, P_1, is observed over the frequency range 1kHz-200kHz and peak, P_2, is discernible in the 100kHz-1MHz range, although it appears as a shoulder on the curve at 1MHz; P_3, also appears as a shoulder on the permittivity response at 35% replacement level and is not discernible at 50% and 65%

replacement. A further feature evident from Figs. 7b and 7c (i.e. 50% and 65% replacement) concerns the response at 1MHz whereby the relative permittivity increases monotonically at times in excess of ~3 hours. This feature is observed, to some extent, at 35% replacement (Fig. 7a) although after ~20-hours, values plateau. Fig. 7b also indicates the regions I-VI identified from the conductivity response presented in Fig. 6c for 50% GGBS. Table 4 presents the $\varepsilon_{r,o}$ values for the GGBS pastes. When compared to Table 3 (0.35 w/b paste), the values are much lower which would be attributable to the reduced ionic concentrations.

(c) Concrete Mixes

Fig. 8a presents the conductivity and Fig. 8b the $d\sigma/dt$ curve for the concrete mixes presented in Table 2; comparative internal temperature measurements for the concretes are presented in Fig.8c. Fig. 9 presents the normalised permittivity. When compared to the respective paste, the addition of aggregate results in a reduction in the absolute values of both conductivity and permittivity (Table 5 presents the $\varepsilon_{r,o}(\omega)$ values for the concretes). When compared to Table 3 (0.45 w/b paste), the values are much lower which is to be expected as the aggregate, itself, will have a low conductivity and permittivity in comparison to that of the paste. However, the features identified from the pastes are still evident in the respective concretes but not as prominent due to a *dilution* effect; regions I-VI discussed above are also distinguishable although they are lengthened in comparison to the pastes due to the slower hydration process resulting from the reduced overall paste content. This indicates that the electrical response of concrete is controlled by the fractional volume of cementitious matrix [28].

INTERPRETATION OF ELECTRICAL RESPONSE

Both the conductivity and the relative permittivity have the potential to reveal information on pore-fluid chemistry, chemical activity on grain surfaces, the formation of hydration

products, hydration kinetics and increase in rigidity of the paste. The following sections interpret the electrical response in terms of physico-chemical and microstructure building processes and in relation to regions I-VI identified above.

(a) CEM I Mixes

The discussion below relates to Figs 3b, 4b and 5b for w/b = 0.35 and are used for illustrative purposes.

Region I: 0-0.5 hour

As the cement is gauged with water, a rapid dissolution (hydrolysis) of ions from the cement grain surfaces takes place, with the different mineralogical phases and calcium sulphate contributing to the pore-solution chemistry of the bulk electrolyte. The aqueous phase contains, primarily, Na^+, K^+, Ca^{2+}, SO_4^{2-} and OH^- which increases with time and is reflected in the rapid increase in the conductivity of the paste in Region I (Fig. 3b).

The permittivity (Fig. 4b) displays a somewhat anomalous response – at low frequencies (1kHz), the permittivity increases, whereas at higher frequencies (>100kHz), it is seen to decrease. On mixing with water, a colloidal suspension is formed and a diffuse electrical double-layer, through adsorbed calcium ions and counterions, will be quickly established on the grain surface. Polarization of the double-layer (Fig. 1a) can induce large dipole moments, hence large permittivity values; however, superimposed upon this process will be electrode polarization effects which can also result in high permittivity values. We are of the opinion that the low-frequency (1kHz) permittivity response is dominated by electrode effects which masks bulk polarization processes; however, the electrode polarization effect must, itself, be

related ionic concentration in the pore water at the specimen/electrode interface [29-31]. As the frequency increases, electrode effects diminish rapidly to reveal the response from the bulk material. Evidence for the rapid reduction in electrode polarization effects comes from the fact that the permittivity decreases by almost three orders of magnitude as the frequency increases from 1kHz-100kHz. However, as the frequency increases from 100kHz-1MHz, ions in the diffuse double-layer find it increasingly more difficult to move in sympathy with the alternations of the electrical field which results in a continual reduction in permittivity with increasing frequency.

The temporal reduction in permittivity at frequencies in the range 100kHz-1MHz would be as a result of the gradual formation and build-up of a gelatinous coating on the cement grain surface reducing ionic mobility in the double layer.

Region II: 0.5 hour – 1.5 hours

Within this region the conductivity continues to increase (Fig. 3b); however, it is noticeable that there is a gradual reduction in $d\sigma/dt$ and the permittivity in the frequency range 100kHz-1MHz continues to decrease with time. This could be explained by invoking two opposing processes:

(i) the continual dissolution of the cement grains which serves to increase the ionic concentration within the bulk pore-fluid, thereby increasing conductivity and low-frequency permittivity (1kHz); and,

(ii) the continual build-up of hydration products on the grain surfaces hindering the dissolution process and removing ions from solution thereby causing a decrease in $d\sigma/dt$ of the paste. The build-up of gel (AFt and C-S-H) on the grain surfaces would

reduce the permittivity (Figs. 4b and 5b) due to reduced ionic mobility in the double layer.

Region III: 1.5 hour – 2.0 hours

This short-lived region displays a marked decrease in conductivity which results in a transitory minimum on the dσ/dt curve (Fig. 3b); over the same period, the permittivity (Fig. 4b) continues to decrease. We are of the opinion that the cause of this feature is as a result of the precipitation of calcium hydroxide. It is noteworthy that this feature has also been observed in dilute suspensions of C_3S with water/solids ratios in the range 5-50 [**32, 33**] and Type I ordinary Portland cement pastes [**11**]. The end of the region is characterized by a reducing rate of change of conductivity (i.e. dσ/dt becomes less negative).

Region IV: 2.0 hours – 6.5 hours

This precipitation process occurring with within region III appears to trigger a decrease in conductivity within region IV and it is over this region that the paste starts to increase in rigidity and the change from an amorphous to crystalline hydrate morphology. It is also evident from Fig. 4b that after approximately 3 hours, the permittivity of the paste increases peaking at approximately 5 hours, which is at a time when the conductivity is undergoing its greatest rate of change. It is also significant that this feature becomes more prominent with increasing frequency of applied field and to highlight this, Fig. 5b presents an enlargement of response at 1MHz. We attribute the increase in polarizability (hence permittivity) of the paste to the nucleation and outgrowth of C-S-H *needles* from C_3S surfaces; this would simultaneously result in,

(i) a more tortuous electrolytic conduction path, thereby decreasing the conductivity; and,

(ii) a rapid (and short-lived) increase in the surface area of the C-S-H which would promote both double-layer polarization processes on the C-S-H surface and, perhaps more significantly, interfacial polarization processes as hydrates grow into the aqueous phase. Hydrate accretion and infilling of the capillary pore space would then serve to reduce the polarizability of the paste.

By the end of this region, a percolated solid phase will have formed.

Region V: 6.5 hours – 9.5 hours

This region is characterised by a *shoulder* in the conductivity response with a resulting peak in the dσ/dt curve (see Fig. 3b). Over the same period, the permittivity curve presented in Fig. 4b also displays a *shoulder* at low-frequencies, however, as the frequency of the applied field increases this changes to a plateau region at 1MHz. On closer examination of the response at 1MHz, this is plateau is a weakly developed peak and indicated, P'_2, on Fig. 5b.

The conductivity curve could be explained by considering the following,

(i) as the cement paste hydrates, its porosity decreases with the pore network becoming more tortuous, constricted and disconnected as a crystalline network is formed. As conduction will be primarily electrolytic in nature via the continuous capillary pores, this will result in a decrease in conductivity; and,

(ii) increasing in ionic concentration within the pore-water which would have the effect of increasing the bulk conductivity. This could be due to the renewed dissolution of the C_3A phase and the formation of ettringite resulting from the reaction of the aluminate phases which releases alkalis bound-up in this phase [34, 35] coupled with the desorption of sulphates from the C-S-H [36].

Considering (i) and (ii), it could be inferred that microstructuaral changes causing a reduction in conductivity, are having a greater influence than changes in pore-fluid chemistry which would increase the conductivity. Release of ions into the pore water would also serve to increase polarizability, hence permittivity [37]. As a pore network has been formed within the paste, in addition to double-layer polarization, interfacial polarization processes (see Fig. 1b) will contribute to the overall polarizability of the paste and causing a transitory increase in permittivity as continuing microstructural changes reduce ionic mobility.

Region VI: 9.5 hours – end of test period

This region is characterised by a continual decrease in conductivity (Fig. 3b) with the rate of change decreasing with increasing hydration time. The permittivity response is, as with region V, frequency dependant – at frequencies <500kHz, the permittivity decreases with time indicting a decrease in polarizability of the paste due to a irrotational binding of double-layer charges. The response at 1MHz (Fig. 5b) reveals an increase in permittivity over this time period, peaking at approximately 11.5 hours (this peak, P_3, is more evident for the paste with w/b = 0.45 in Fig. 5a). The increase in polarizability could be attributed to increased interfacial processes at crystal boundary interfaces within the pore structure (Fig. 1b) resulting from an increase in ionic concentrations in the pore fluid. Interfacial polarization is a higher frequency process than double-layer effects hence only become more prominent as the frequency increases. As with Region V, this could be as a result of the transformation of AFt to AFm with the release of Ca^{2+} and SO_4^{2-} (Eq 6) and reaction on the C_3A phases (Eq 7) releasing alkalis bound up in them:

$$C_6A\bar{S}_3H_{32} \rightarrow C_4A\bar{S}H_{12} + 2CaSO_4 \quad (6)$$

$$C_6A\bar{S}_3H_{32} + 2C_3A + 4H \rightarrow 3C_4A\bar{S}H_{12} \quad (7)$$

There is no detectable increase in conductivity caused by release of ions into the pore network so it could be inferred that microstructural changes in the pore network due to hydration are now having a more dominant influence on the conductivity of the paste than changes in pore-fluid chemistry.

(b) GGBS mixes

The electrical response of the GGBS presented in Figs. 6 and 7 is similar in many aspects to the response for the Portland cement pastes as six regions can also be identified during the initial 24-hours after gauging. However, as noted above, the duration of some of the regions identified from the conductivity response (and its derivative) are increased in comparison to the pure cement paste (in particular, regions III and V). For illustrative purposes, Fig. 6c identifies the regions for the 50% GGBS (w/b=0.35) from the conductivity response and Fig. 7b presents the permittivity with regions I-VI indicated. The most striking difference between the pure cement paste and the GGBS pastes concerns the permittivity response, and the following should be noted:

(i) the merging of peaks P_2 (reaction on C_3S phase and CSH formation) and P'_2 (renewed dissolution on the C_3A phase and AFt formation) into a single broader peak spanning across regions IV and V; and,

(ii) within regions V and VI, at 500kHz and 1MHz, the polarizability of the paste increases with time, and is particularly evident at 1MHz (Note: right-hand axis for 1MHz scale). As before, at these higher frequencies we attribute this to an increase in interfacial polarization effects resulting from the AFt$\rightarrow$AFm transformation and subsequent release of ions into the pore water. At frequencies <200kHz, the polarizability of the paste will be dominated by double-layer polarization processes which will decrease

with time due to densification of the crystalline network and consequent reduction in charge mobility.

(c) Concrete Mixes

Fig. 8a presents the temporal change in the conductivity over the initial 24-hours hydration, with the corresponding derivative presented in Fig. 8b. It is immediately evident that the key features identified from the pastes earlier are still visible, albeit much less pronounced. It is also evident the absolute values of conductivity of the concrete mixes are considerably lower than those of the respective pastes - decreasing by a factor of approximately 6. This simply reflects the *diluting* effect of the aggregate reducing the volume fraction of cement-paste. The derivative curves presented in Fig. 8b is also similar to those observed earlier from the pastes (see Figs. 3a and 6b). The features of the normalised permittivity presented in Figs. 9a–9c compare well with those observed from the paste samples (see Figs. 4c and 7a-7c) although absolute values of permittivity are much reduced (see Table 5).

CONCLUDING REMARKS

Conductivity and permittivity measurements have been presented over the frequency range 1kHz-1MHz for cement pastes and concretes, with and without GGBS replacement. Work focussed on the initial 24-hours after mixing with water and it was shown that the response at the permittivity level was frequency-dependent and related to polarization processes within the cementitious matrix. Permittivity measurements decreased by over four orders of magnitude as the frequency increased from 1kHz to 1MHz and features of the permittivity response, which were masked at low frequencies, only revealed themselves at higher frequencies. Over this frequency range, the main polarization processes operative were electrode polarization which was dominant at frequencies less than 10kHz, whereas double-

layer polarization and interfacial polarization dominated in the 100kHz-1MHz frequency range. Over the frequency range 100kHz-1MHz, the conductivity increased by less than 15%, the increase being due to the relaxation of bulk polarization processes.

During the initial 24-hours after mixing with water, six regions could be identified from both conductivity and permittivity measurements with measurements explained in terms of through-solution mechanisms (i.e. dissolution, precipitation), C-S-H and AFt formation and AFt to AFm transformation. It was also shown that concrete mixes exhibit similar features to those of the respective pastes, although the absolute values are consistently much lower which can be attributed to the diluting effect of the low-conductivity and low-permittivity aggregate.

The methodology can be equally applied to concretes and there is considerable scope for development of multi-frequency impedance measurements within the range 10kHz-1MHz as an additional testing technique to study the early hydration of cementitious materials generally. Furthermore, the work allows optimization of the frequency at which electrical impedance measurements are most informative with regard to hydration and microstructural development.

ACKNOWLEDGEMENTS

The Authors wish to thank Hanson Cement (UK) for supplies of GGBS. HMT wishes to acknowledge the financial support provided by Heriot Watt University through a James Watt Scholarship.

REFERENCES

[1] McCarter, W. J. and Curran, P., "The electrical response of setting cement paste," *Mag. Conc. Res*., Vol. 36, No. 126, 1984, pp 42-49.

[2] McCarter, W. J. and Afshar, A. B., "Some aspects of the electrical properties of cement paste,", *J. Matl. Sci. Lett*., Vol. 3, 1984, pp. 1083-1086.

[3] McCarter, W. J. and Afshar, A., "A Study of the Early hydration of Portland Cement," *Proc. Instn. Civ. Engrs. (London)*, Pt. 2, No. 79, Sept., 1985, pp. 585-604.

[4]Torrents, J. M., Roncero, J., and Gettu, R., "Utilization of Impedance Spectroscopy for Studying the Retarding Effect of a Superplasticizer on the Setting of Cement," *Cem. Concr. Res.*, Vol. 28, No. 9, 1998, pp. 1325–1333.

[5] Morsy, M. S., "Effect of Temperature on Electrical Conductivity of Blended Cement Pastes," *Cem. Concr. Res.*, Vol. 29, No. 4, 1999, pp. 603–606.

[6] Levita, G., Marchetti, A., Gallone, G., Princigallo, A., and Guerrini, G. L., "Electrical Properties of Fluidified Portland Cement Mixes in the Early Stage of Hydration," *Cem. Concr. Res.*, Vol. 30, No. 6, 2000, pp. 923–930.

[7] Salem, Th. M., "Electrical Conductivity and Rheological Properties of Ordinary Portland Cement–silica Fume and Calcium Hydroxide–silica Fume Pastes," *Cem. Concr. Res.*, Vol. 32, No. 9, 2002, pp. 1473–1481.

[8] Princigallo, A., van Breugel, K., and Levita, G., "Influence of the Aggregate on the Electrical Conductivity of Portland Cement Concretes," *Cem. Concr. Res.*, Vol. 33, No. 11, 2003, pp. 1755–1763.

[9] Heikal, M., Morsy, M. S., and Radwan, M. M., "Electrical Conductivity and Phase Composition of Calcium Aluminate Cement containing Air-cooled and Water-cooled Slag at 20, 40 and 60°C," *Cem. Concr. Res.*, Vol. 35, No. 7, 2005, pp. 1438–1446.

[10] Wei, X. and Li, Z., "Early Hydration Process of Portland Cement Paste by Electrical Measurement," *ASCE J. Mater. Civ. Eng.*, Vol. 18, No. 1, 2006, pp. 99–105.

[11] Rajabipour, F., Sant, G., and Weiss, J., "Development of Electrical Conductivity-Based Sensors for Health Monitoring of Concrete Materials," TRB Annual Conference, CD-ROM Paper#07-1765 (16 pages), Transportation Research Board, Washington DC, 2007, http://web.archive.org/web/20161107132357/https://trid.trb.org/view.aspx?id=801858 (accessed November 7th 2016).

[12] Xiao, L. and Li, Z., "Early-age Hydration of Fresh Concrete Monitored by Non-contact Electrical Resistivity Measurement," *Cem. Concr. Res.*, Vol. 38, No. 3, 2008, pp. 312–319.

[13] Zhang, J., Qin, L., and Li, Z., "Hydration and Monitoring of Cement-based Materials with Resistivity and Ultrasonic Methods," *Mater. Struct.*, Vol. 42, No. 1, 2009, pp. 15–24.

[14] Topçu, İ. B., Uygunoğlu, T., and Hocaoğlu, İ., "Electrical Conductivity of Setting Cement Paste with Different Mineral Admixtures," *Constr. Build. Mater.*, Vol. 28, No. 1, 2012, pp. 414–420.

[15] Sanish, K.B., Neithalath, N., and Santhanam, M., "Monitoring the Evolution of Material Structure in Cement Pastes and Concretes using Electrical Property Measurements," *Constr. Build. Mater.*, Vol. 49, No. December, 2013, pp288-297.

[16] Tang, S. W., Cai, X. H., He, Z., Shao, H. Y., Li, Z. J., and Chen, E., "Hydration Process of Fly Ash Blended Cement Pastes by Impedance Measurement," *Constr. Build. Mater.*, Vol. 113, No. 15, 2016, pp. 939–950.

[17] Gorur, K., Smit, M. K., and Wittmann, F. H., "Microwave Study of Hydrating Cement Paste at Early Age," *Cem. Concr. Res.*, Vol. 12, No. 4, 1982, pp. 447–454.

[18] Moukwa, M., Brodwin, M., Christo, S., Chang, J., and Shah, S. P., "The Influence of the Hydration Process upon Microwave Properties of Cements," *Cem. Concr. Res.*, Vol. 21, No. 5, 1991, pp. 863–872.

[19] Zhang, X., Ding, X. Z., Ong, C. K., Tan, B. T. G., and Yang, J., "Dielectric and Electrical Properties of Ordinary Portland Cement and Slag Cement in the Early Hydration Period," *J. Mater. Sci.*, Vol. 31, No. 5, 1996, pp. 1345–1352.

[20] Zhang, X., Yang, Y., and Ong, C. K., "Correlation of Microwave and Conduction Calorimeter Measurements on the Hydration of Cement," *J. Mater. Sci. Let.*, Vol. 16, No. 23, 1997, pp. 1885–1887.

[21] Smith, A., Abélard, P., Thummen, F., and Allemand, A., "Electrical Characterisation as a Function of Frequency: Application to Aluminous Cement during Early Hydration," *Cem. Concr. Compos.*, Vol. 24, No. 5, 2002, pp. 477–484 .

[22] British Standards Institution (BSI), EN197-1:2000, *Cement-Part 1: Composition, Specifications and Conformity Criteria for Common Cements*, BSI, London, 2000.

[23] British Standards Institution (BSI), EN15167-1:2006, *Ground Granulated Blast Furnace Slag for Use in Concrete, Mortar and Grout – Part 1: Definitions, Specifications and Conformity Criteria*, BSI, London, 2006.

[24] Schwan, H. P., Schwarz, G., Maczuk, J., and Pauly, H., "On the Low-frequency Dielectric Dispersion of Colloidal Particles in Electrolyte Solution," *J. Phys. Chem.*, Vol. 66, No. 12, 1962, pp. 2626–2635.

[25] Schwarz, G., "A Theory of the Low-frequency Dielectric Dispersion of Colloidal Particles in Electrolyte Solution," *J. Phys. Chem.*, Vol. 66, No. 12, 1962, pp. 2636–2642.

[26] Hasted, J. B., *Aqueous Dielectrics*, Chapman and Hall, London, 1973.

[27] McCarter, W. J., Tran, D., “Monitoring Pozzolanic Activity by Direct Activation with Calcium Hydroxide,” *Constr. Build. Mater.*, Vol. 10, No. 3, 1996, pp179-184.

[28] Whittington, H. W., McCarter, J., and Forde, M. C., “The Conduction of Electricity through Concrete,” *Mag. Concr. Res.*, Vol. 33, No. 114, 1981, pp. 48–60.

[29] Bordi, F., C. Cametti, and T. Gili, “Reduction of the Contribution of Electrode Polarization Effects in the Radiowave Dielectric Measurements of Highly Conductive Biological Cell Suspensions, ” *Bioelectrochemistry*, Vol. 54, No. 1, 2001, pp53-61.

[30] Ishai, P. B., Talary, M. S., Caduff, A., Levy, E., and Feldman, Y., “Electrode Polarization in Dielectric Measurements: a Review, ” *Meas. Sci. Tech.*, Vol. 24, No. 10, 2013, 102001 (21pp) (doi: 0957-0233/24/10/102001).

[31] Serghei, A., Tress, M., Sangoro, J. R., and F. Kremer, “Electrode Polarization and Charge Transport at Solid Interfaces,” *Phys. Rev. B*, Vol. 80, No. 18, 2009, pp184301-1/5 (doi: 10.1103/PhysRevB.80.184301).

[32] Bazzoni, A., Ma, S., Wang, Q., Shen, X., Cantoni, M., and Scrivener, K. L., “The Effect of Magnesium and Zinc Ions on the Hydration Kinetics of C_3S,” *J. Am. Ceram. Soc.*, Vol. 97, No. 11, 2014, pp. 3684–3693.

[33] Sowoidnich, T., *A Study of Retarding Effects on Cement and Tricalcium Silicate Hydration Induced by Superplasticizers*, PhD Thesis, Bauhaus-Universität Weimar, 2015.

[34] Odler, I, and Wonnemann, R., “Effect of Alkalies on Portland Cement Hydration: I. Alkali Oxides incorporated into the Crystalline Lattice of Clinker Minerals,” *Cem. Concr. Res.*, Vol. 13, No. 4, 1983, pp. 477–482.

[35] Gartner, E. M., Young, J. F., Damidot, D. A., and Jawed, I., “Hydration of Portland Cement,” *Structure and Performance of Cements*, *Chapter 3*, J. Bensted and P. Barnes, Eds., 2nd Edition, Spon Press, London, 2002 (ISBN 0-419-23330-X).

[36] Scrivener, K. L., Juilland, P., and Monteiro, P. J. M., “Advances in Understanding Hydration of Portland Cement,” *Cem. Concr. Res.*, Vol. 78 (Part A), 2015, pp. 38–56.

[37] Chen, Y., and Or, D., “Effects of Maxwell-Wagner Polarization on Soil Complex Dielectric Permittivity Under Variable Temperature and Electrical Conductivity,” *Water Resources Research*, Vol. 42, No. 6, 2006, W06424-1/14 (doi:10.1029/2005WR004590).

Table 1: Oxide Analysis of Cementitious Materials.

By weight %	CEM I	GGBS
SiO_2	20.95	33.89
AI_2O_3	5.2	13.96
Fe_2O_3	3.42	0.35
CaO	59.86	38.03
MgO	2.25	8.77
K_2O	0.56	0.67
Na_2O	0.21	0.24

Table 2: Concrete mixes used in experimental program.

Mix	w/b	CEM I kg/m^3	GGBS kg/m^3	20mm kg/m^3	10mm kg/m^3	Fine (<4mm) kg/m^3
PCC	0.45	339	0	781	390	781
GGBS35	0.45	220	118	778	389	778
GGBS65	0.45	118	219	776	388	776

Table 3: Initial permittivity values ($\varepsilon_{r,o}(\omega)$) for cement pastes at frequencies presented in Fig. 4.

w/b	1kHz	100kHz	200kHz	500kHz	1MHz
0.30	9.55×10^6	9.06×10^3	2.76×10^3	8.90×10^2	4.04×10^2
0.35	8.01×10^6	9.28×10^3	3.45×10^3	1.05×10^3	5.32×10^2
0.45	7.59×10^6	1.25×10^4	4.12×10^3	9.70×10^2	3.96×10^2

Table 4: Initial permittivity values ($\varepsilon_{r,o}(\omega)$) for GGBS pastes at frequencies presented in Fig. 7.

w/b	1kHz	100kHz	200kHz	500kHz	1MHz
35% GGBS	6.50×10^6	5.46×10^3	1.72×10^3	3.47×10^2	97.5
50% GGBS	6.03×10^6	4.59×10^3	1.45×10^3	2.84×10^3	70.7
65% GGBS	4.76×10^6	1.96×10^3	6.12×10^2	1.04×10^2	14.2

Table 5: Initial permittivity values ($\varepsilon_{r,o}(\omega)$) for concretes presented in Fig. 9.

	1kHz	100kHz	200kHz	500kHz	1MHz
PC	2.11×10^5	1.25×10^2	81.6	33.3	19.2
GGBS35	1.27×10^5	1.02×10^2	93.3	55.1	36.4
GGBS65	6.62×10^4	54.3	55.1	31.7	23.7

Captions for Figures

Fig. 1 Schematic diagram showing (a) Double-layer polarization, and (b) Interfacial (or space-charge) polarization.

Fig. 2 (a) Conductivity response during initial 24-hours for CEM I cement pastes, (b) enlargement showing initial 2.5 hours after mixing (Note: legend as in (a)), and (c) variation in internal temperature of CEM I cement pastes.

Fig. 3 (a) Derivative of curves in Fig. 2(a), and (b) conductivity and derivative for w/b = 0.35 paste indicating Regions I-VI.

Fig. 4 Normalized permittivity at frequencies shown in Figure legend for CEM I pastes (a) w/b = 0.3, (b) w/b = 0.35, and (c) w/b = 0.45

Fig. 5 Normalized permittivity (1MHz) for CEM I pastes (a) w/b = 0.30, 0.35 and 0.45, and (b) w/b = 0.35 showing Regions I-VI and weakly developed peak, P'_2.

Fig. 6 (a) Conductivity response during initial 24-hours for GGBS pastes,(b) derivative of curves in (a), (c) conductivity and derivative for 50% GGBS paste indicating Regions I-VI, and (d) variation in internal temperature of GGBS pastes.

Fig. 7 Normalized permittivity for GGBS pastes (a) 35%, (b) 50% with Regions I-VI indicated, and (c) 65%. (Note: Use right-hand axis for 1MHz curve; legend shown in (b)).

Fig. 8 (a) Conductivity response during initial 24-hours for concretes in Table 2, (b) derivative of curves in (a), and (c) variation in internal temperature of concretes.

Fig. 9 Normalized permittivity for concretes in Table 2 (a) PCC, (b) GGBS35, and (c) GGBS65. (Note: Legend shown in (b)).

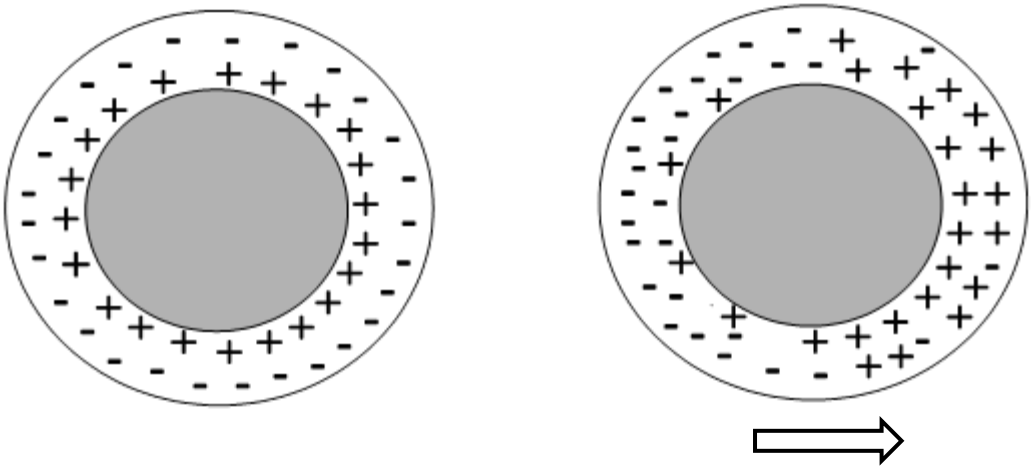

No Field (E = 0) Applied Field E ≠ 0)

(a)

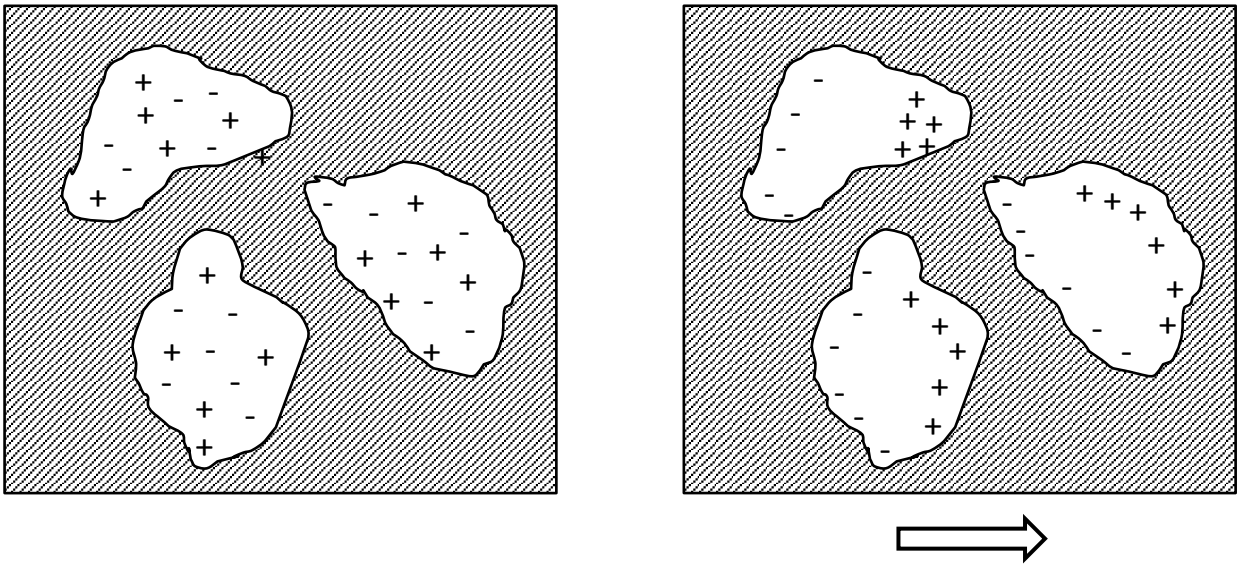

No Field (E = 0) Applied Field (E ≠ 0)

(b)

Fig. 1

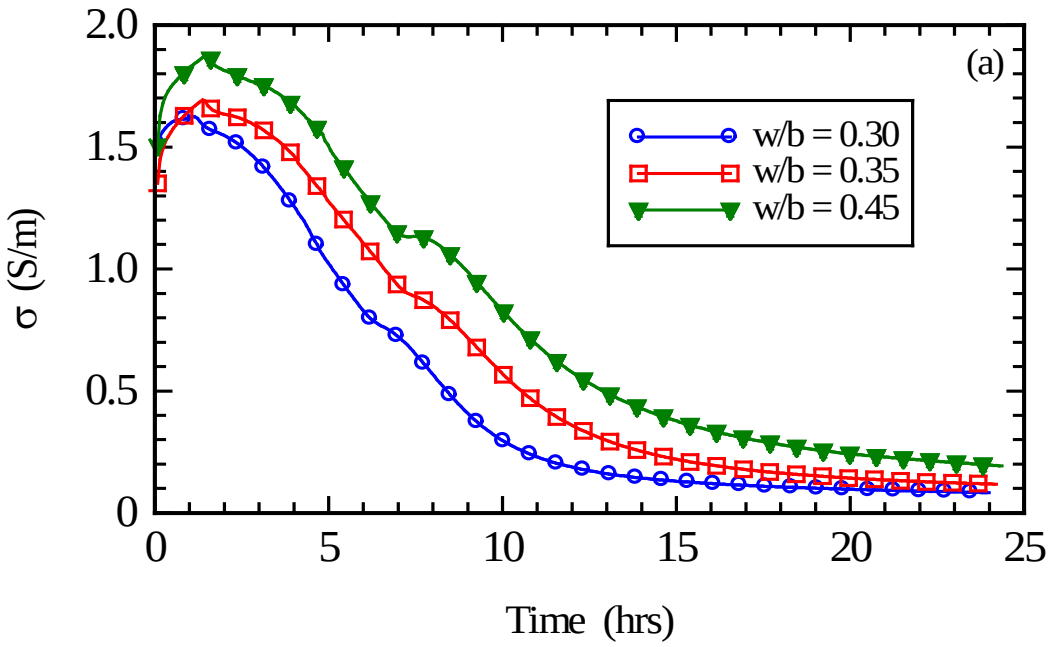
(a)
w/b = 0.30
w/b = 0.35
w/b = 0.45
σ (S/m)
Time (hrs)
2.0
1.5
1.0
0.5
0
0
5
10
15
20
25

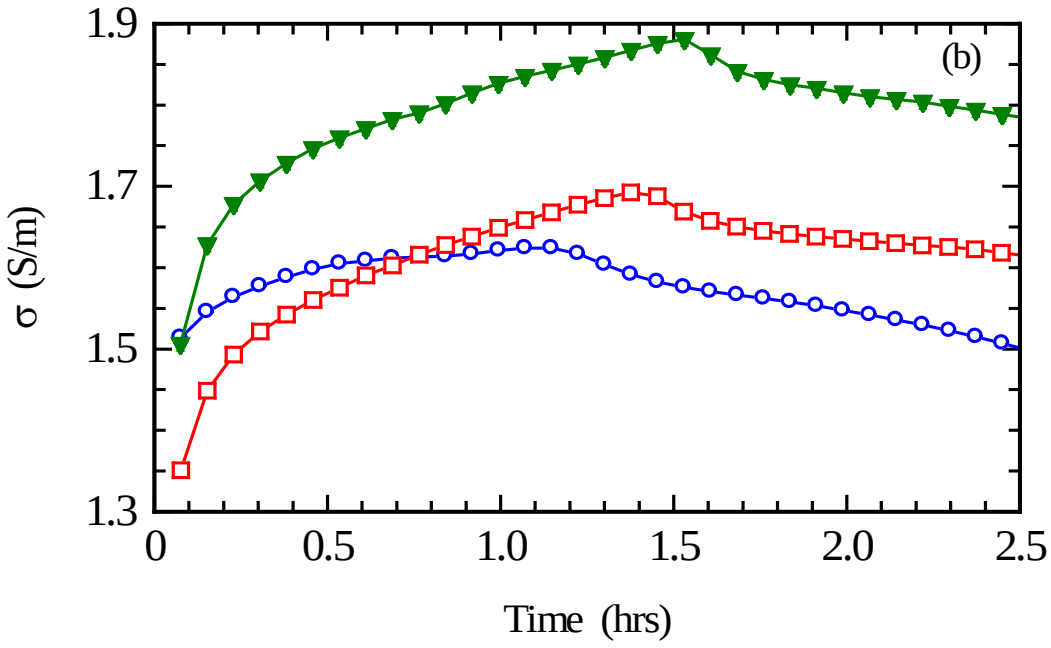
(b)
σ (S/m)
Time (hrs)
1.9
1.7
1.5
1.3
0
0.5
1.0
1.5
2.0
2.5

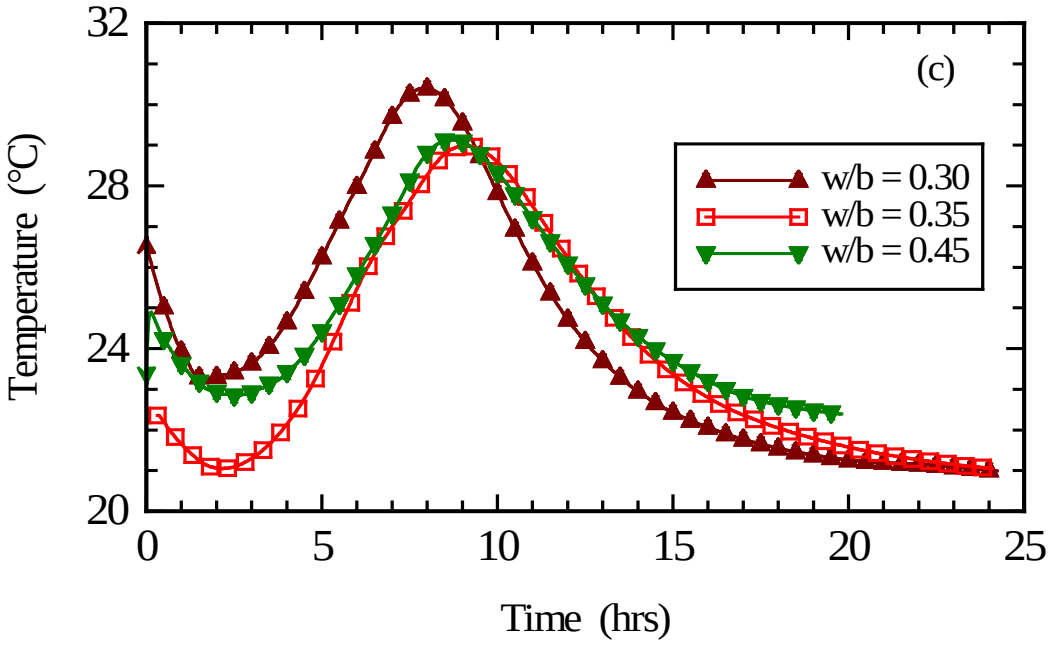
(c)
w/b = 0.30
w/b = 0.35
w/b = 0.45
Temperature (°C)
Time (hrs)
32
28
24
20
0
5
10
15
20
25

FIG. 2

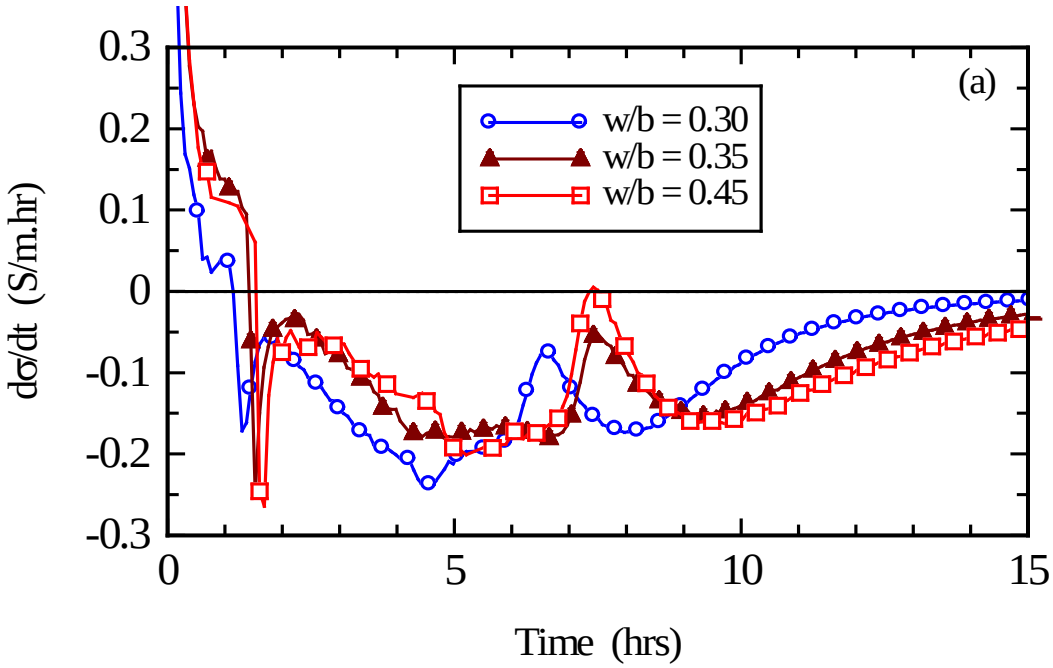
0.3
0.2
0.1
0
-0.1
-0.2
-0.3
0
5
10
15
dσ/dt (S/m.hr)
Time (hrs)
(a)
w/b = 0.30
w/b = 0.35
w/b = 0.45

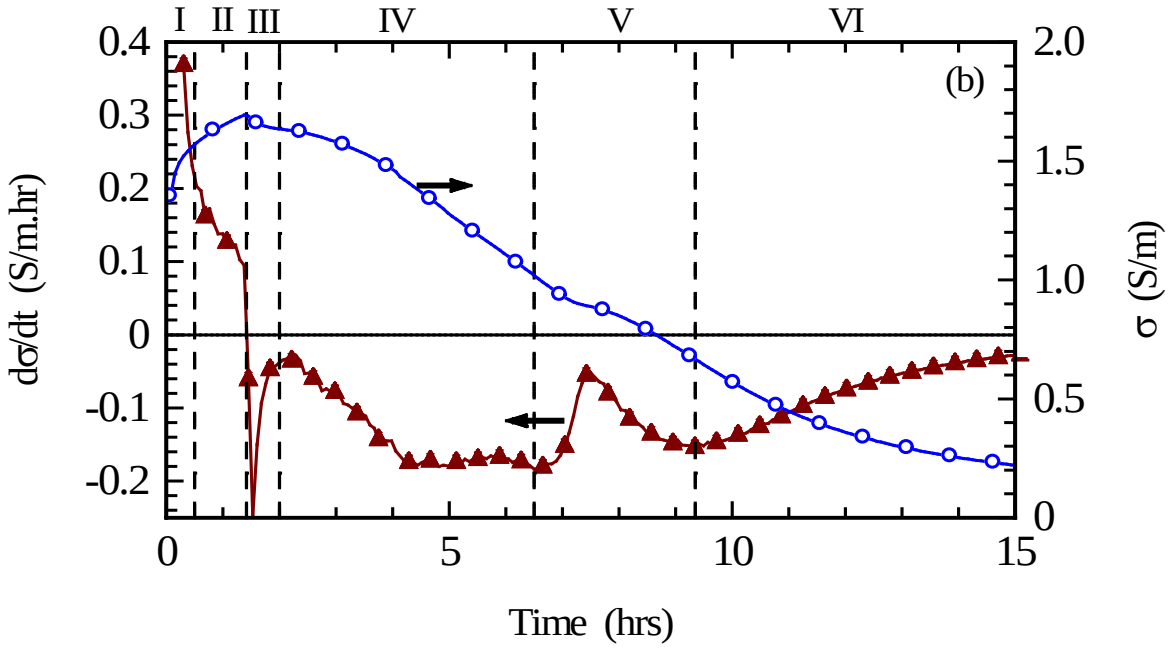
I
II
III
IV
V
VI
0.4
0.3
0.2
0.1
0
-0.1
-0.2
2.0
1.5
1.0
0.5
0
0
5
10
15
dσ/dt (S/m.hr)
σ (S/m)
Time (hrs)
(b)

FIG. 3

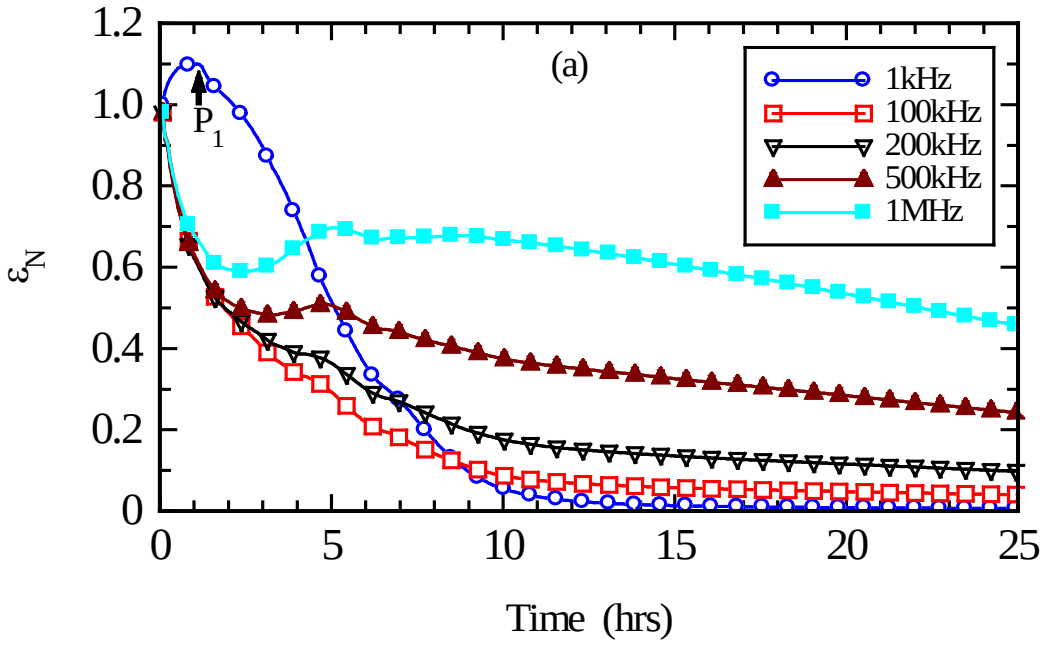
(a)
1kHz
100kHz
200kHz
500kHz
1MHz
P1
εN
Time (hrs)
0
0.2
0.4
0.6
0.8
1.0
1.2
0
5
10
15
20
25

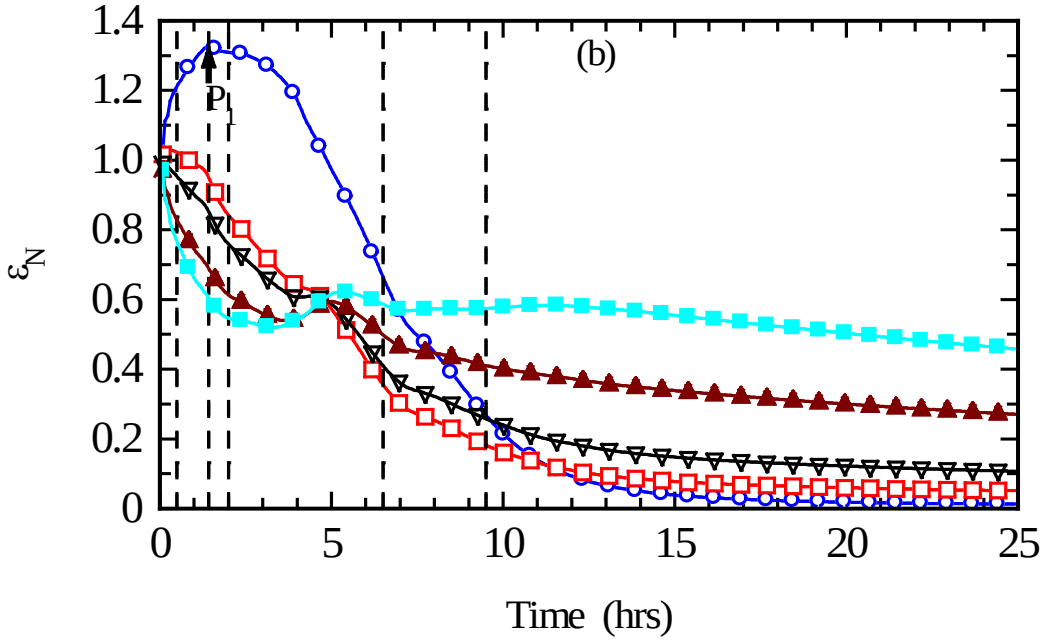
(b)
P1
εN
Time (hrs)
0
0.2
0.4
0.6
0.8
1.0
1.2
1.4
0
5
10
15
20
25

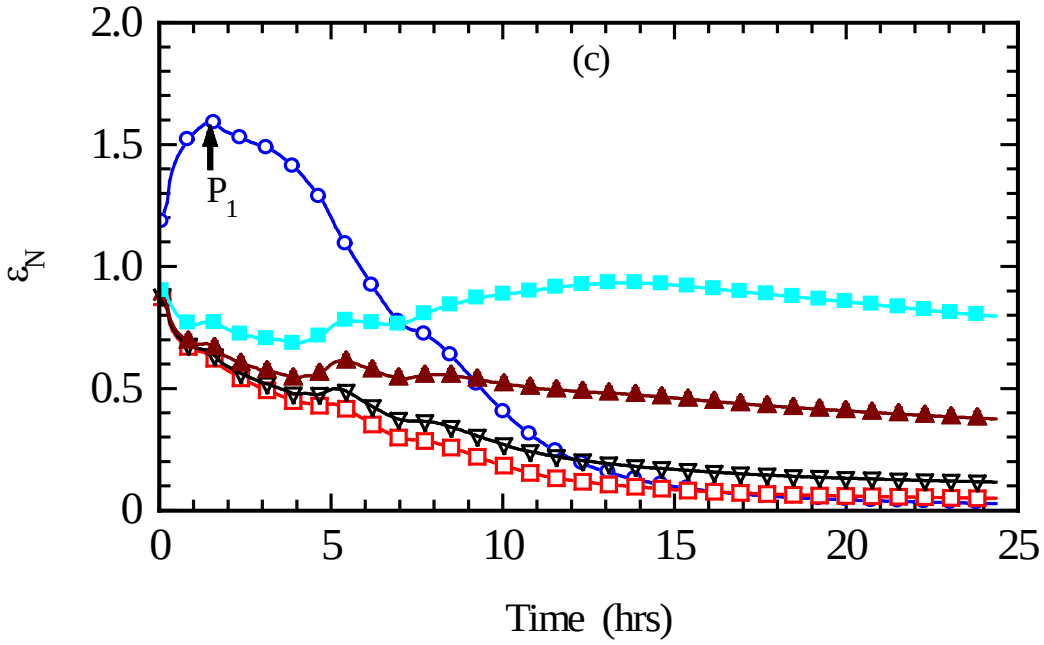

FIG. 4

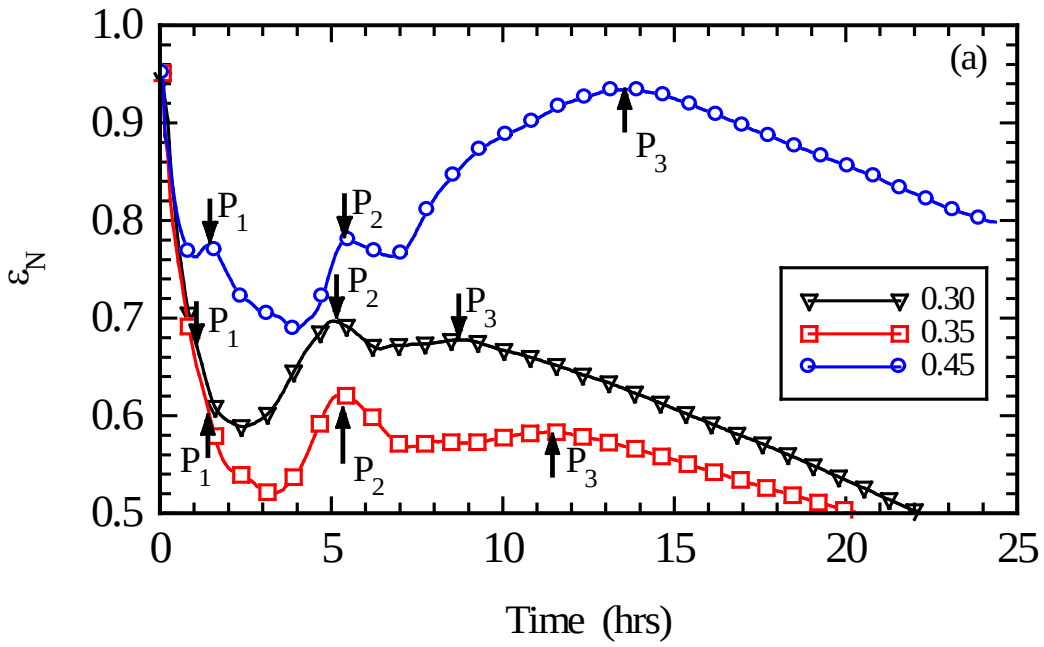
(a)
ε_N
Time (hrs)
0.30
0.35
0.45
P1
P2
P3

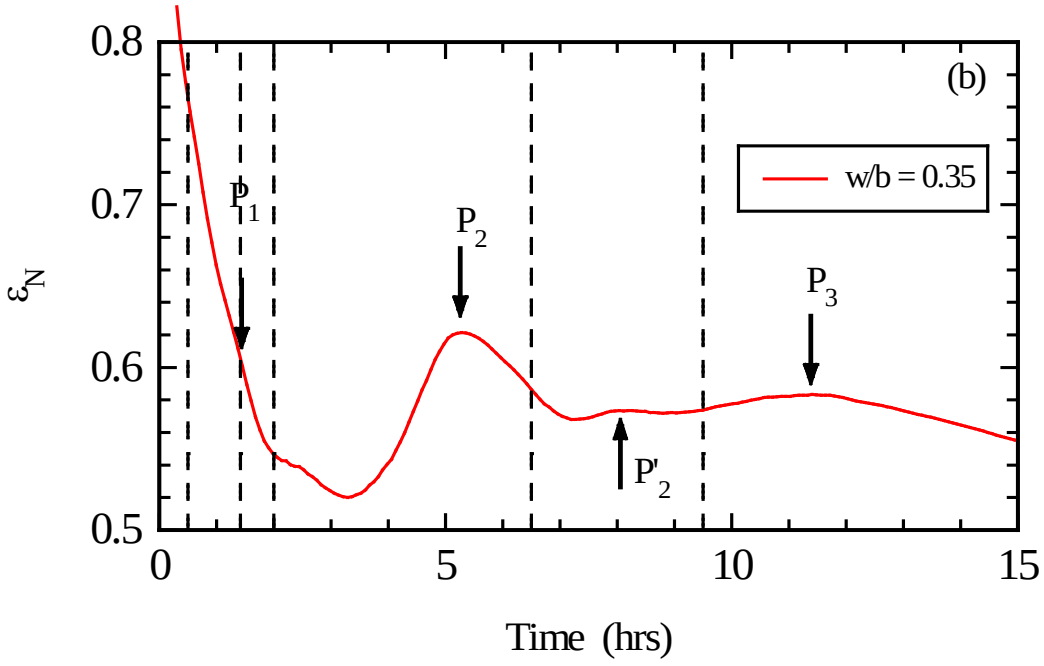
(b)
ε_N
Time (hrs)
w/b = 0.35
P1
P2
P3
P'2

FIG. 5

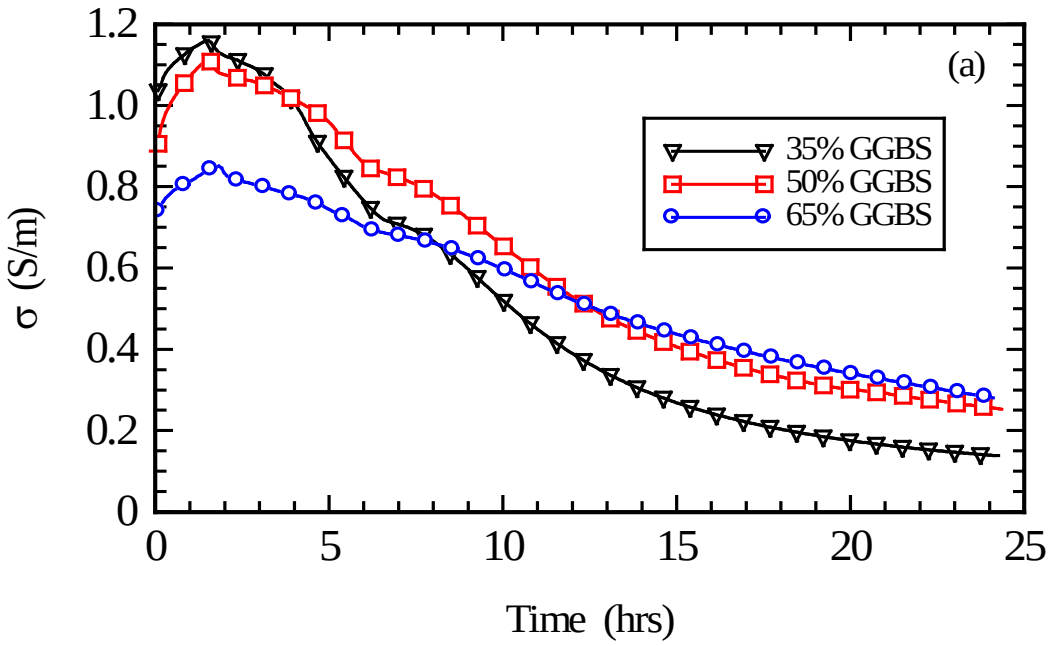
(a)
35% GGBS
50% GGBS
65% GGBS
σ (S/m)
Time (hrs)
0
0.2
0.4
0.6
0.8
1.0
1.2
0
5
10
15
20
25

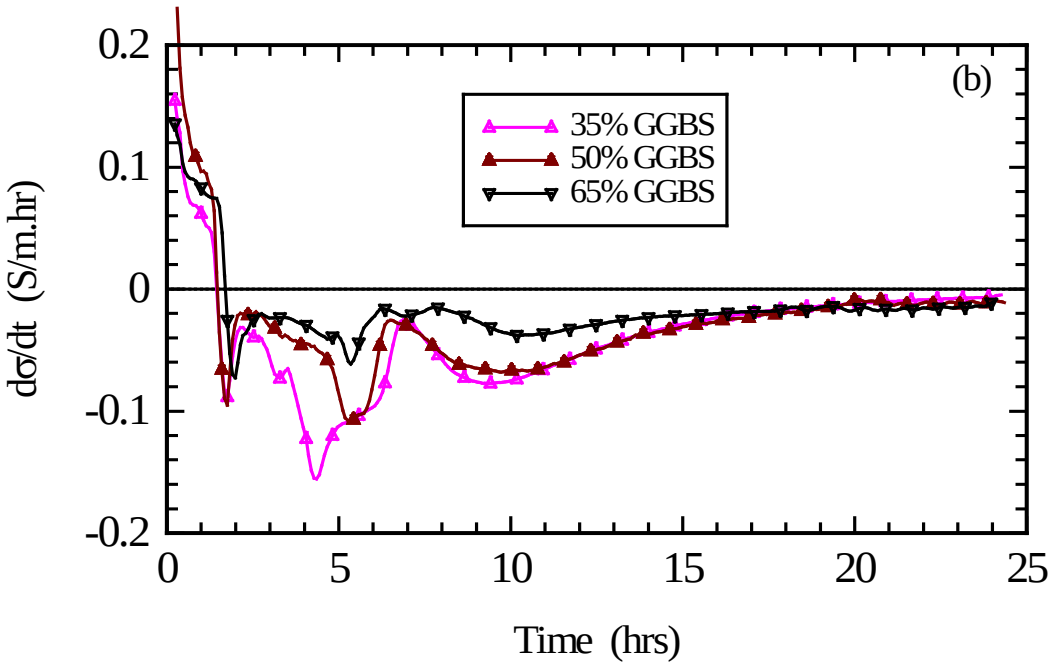
(b)
35% GGBS
50% GGBS
65% GGBS
dσ/dt (S/m.hr)
Time (hrs)
0.2
0.1
0
-0.1
-0.2
0
5
10
15
20
25

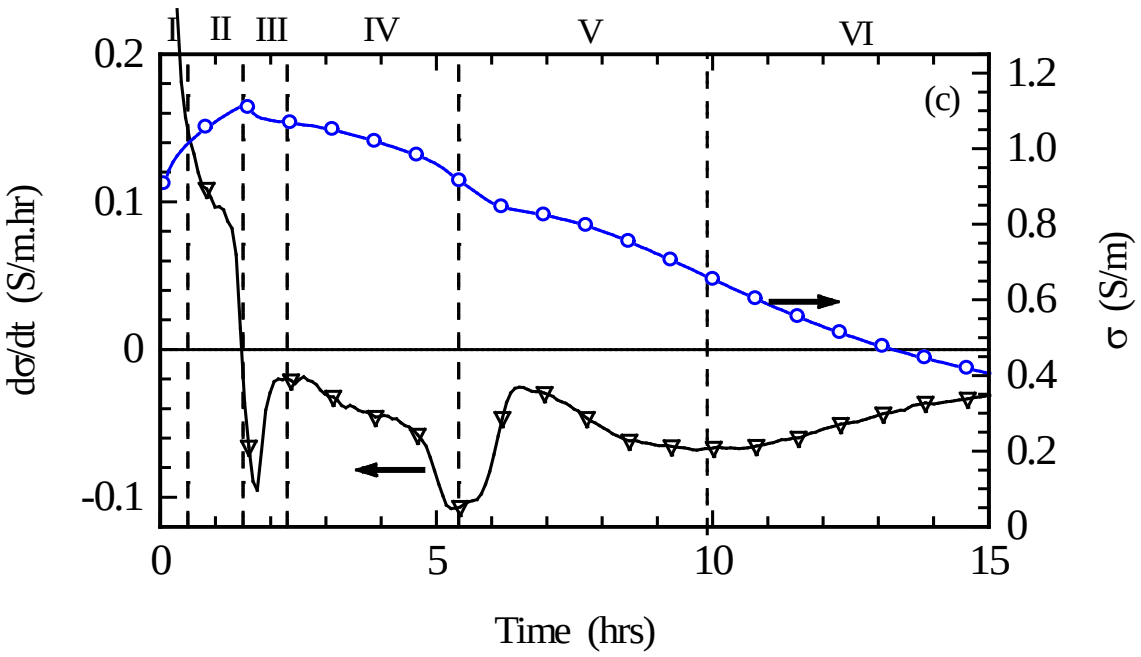
I
II
III
IV
V
VI
(c)
dσ/dt (S/m.hr)
σ (S/m)
Time (hrs)

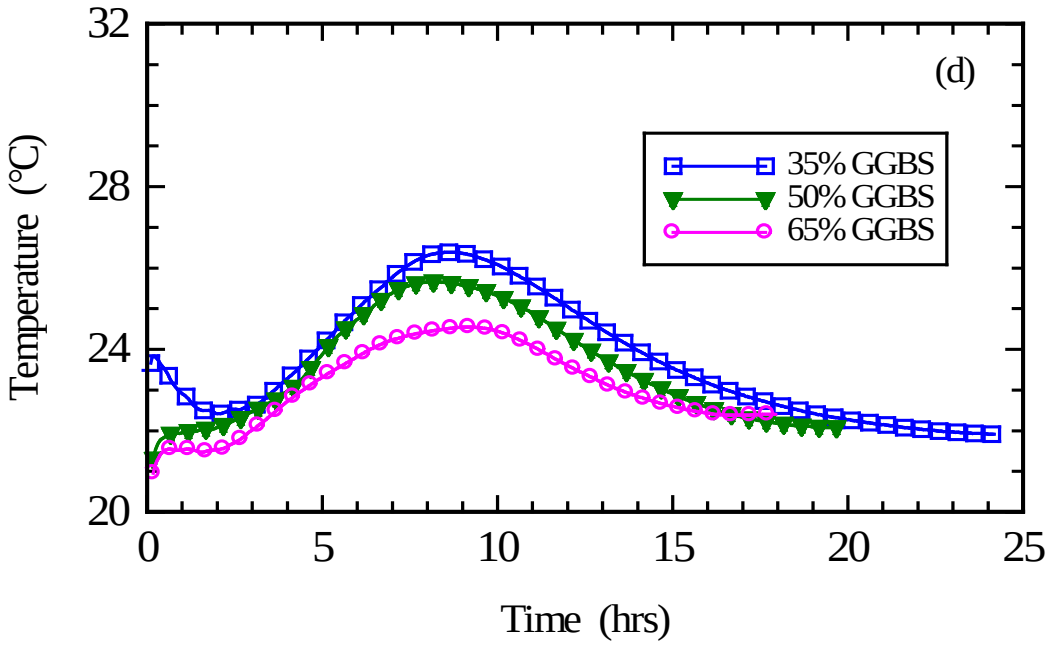
(d)
35% GGBS
50% GGBS
65% GGBS
Temperature (°C)
Time (hrs)

FIG. 6

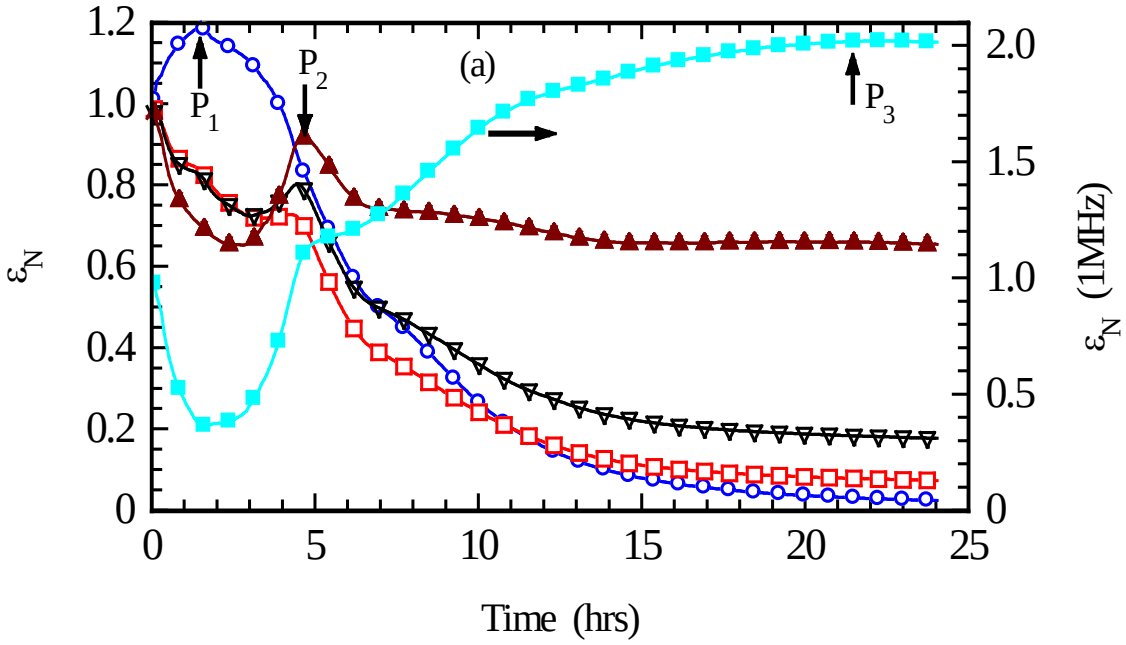
(a)
P1
P2
P3
εN
εN (1MHz)
Time (hrs)

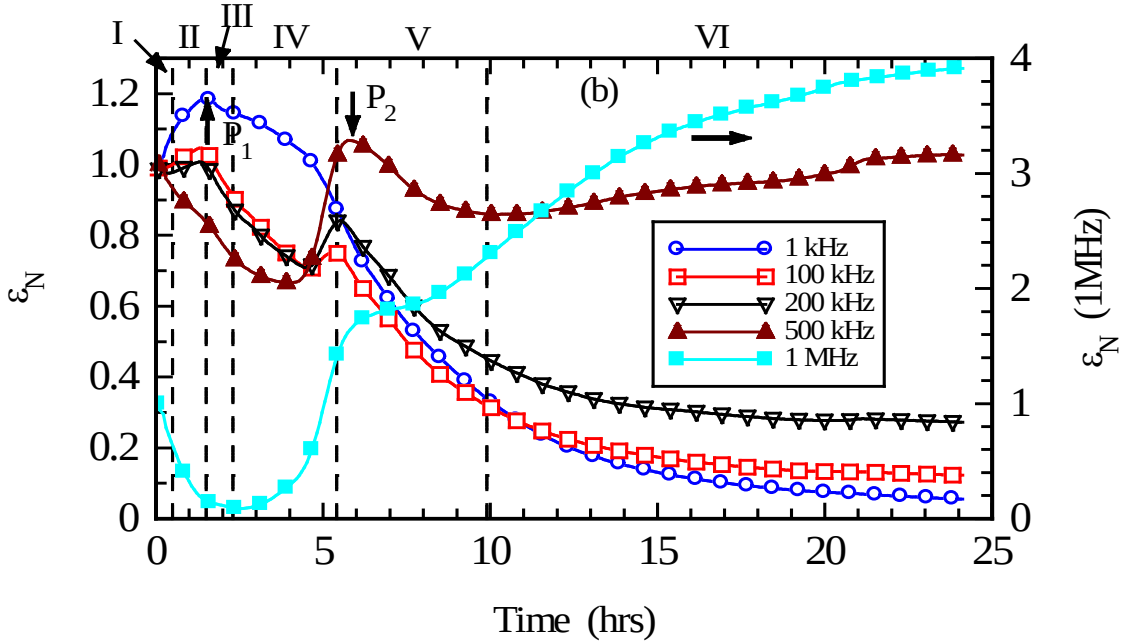
I
II
III
IV
V
VI
(b)
P1
P2
1 kHz
100 kHz
200 kHz
500 kHz
1 MHz
εN
εN (1MHz)
Time (hrs)

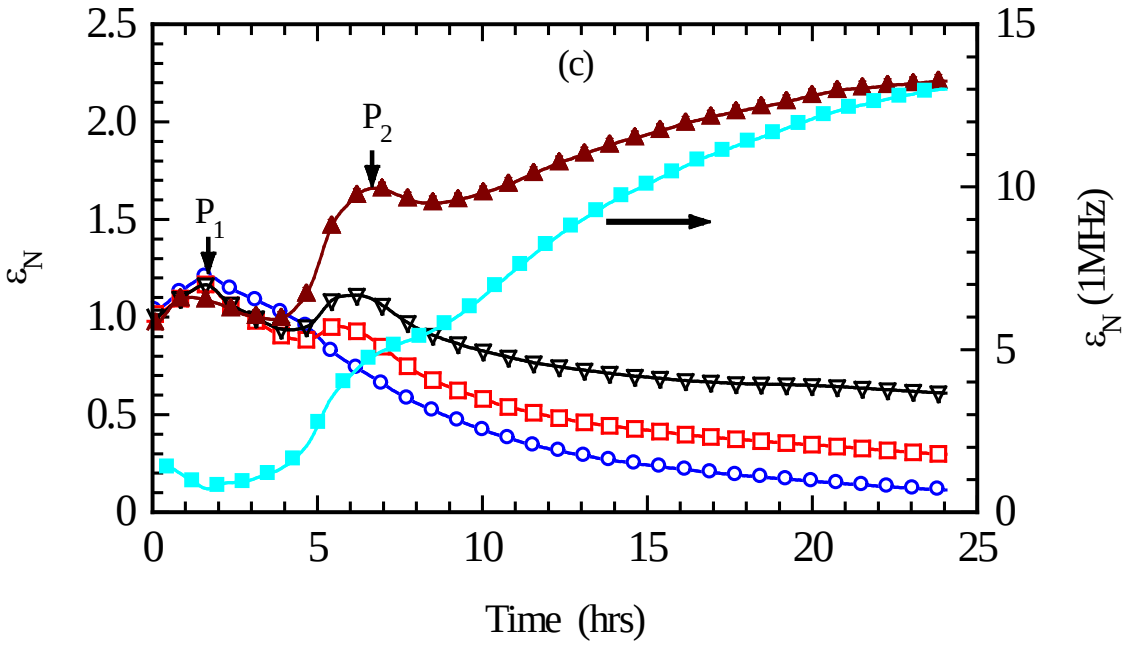

FIG. 7

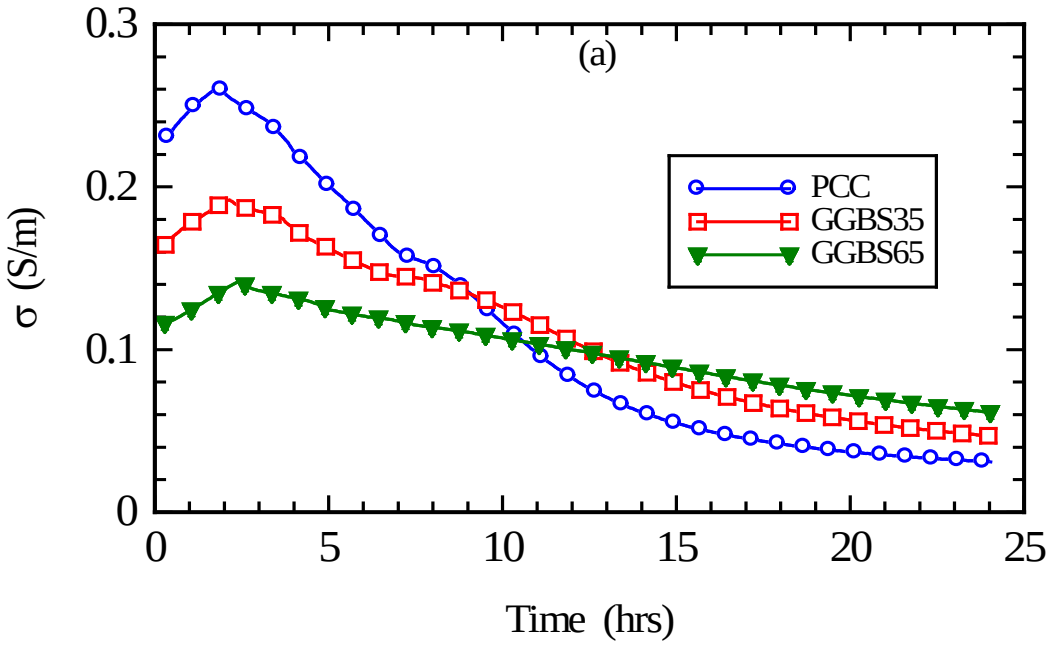
(a)
PCC
GGBS35
GGBS65
σ (S/m)
Time (hrs)
0.3
0.2
0.1
0
0
5
10
15
20
25

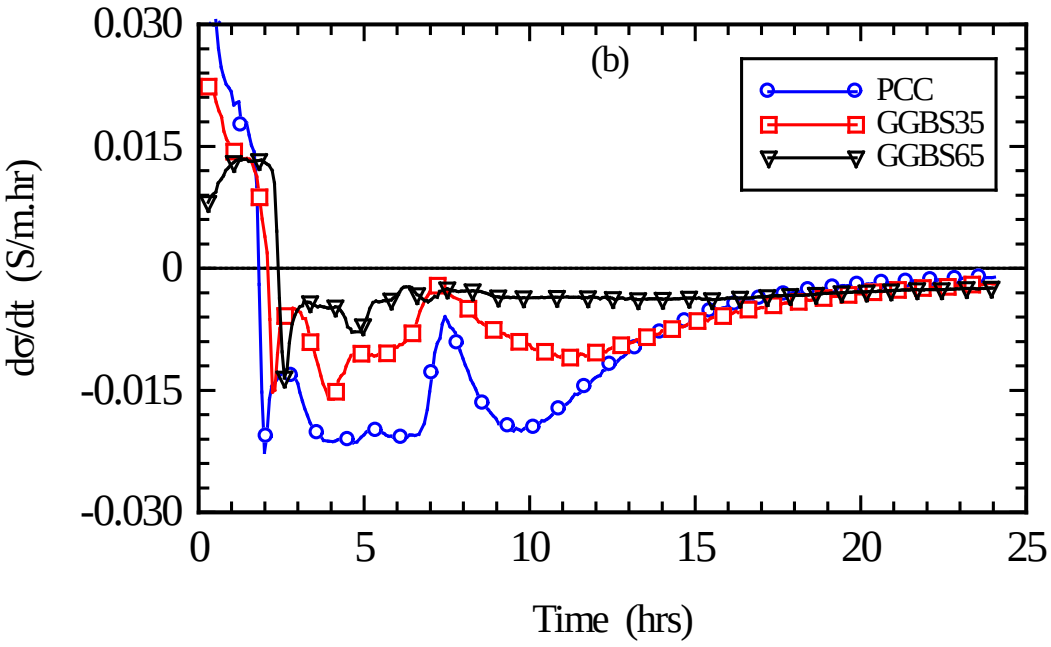
(b)
PCC
GGBS35
GGBS65
dσ/dt (S/m.hr)
Time (hrs)
0.030
0.015
0
-0.015
-0.030
0
5
10
15
20
25

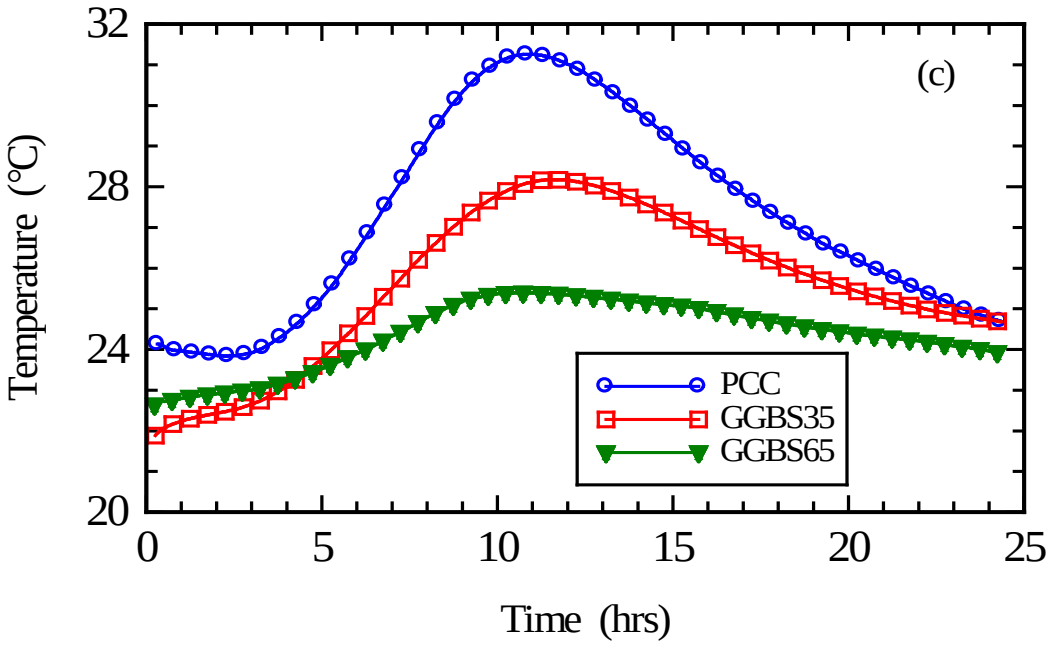
32
28
24
20
Temperature (°C)
0
5
10
15
20
25
Time (hrs)
(c)
PCC
GGBS35
GGBS65

FIG. 8

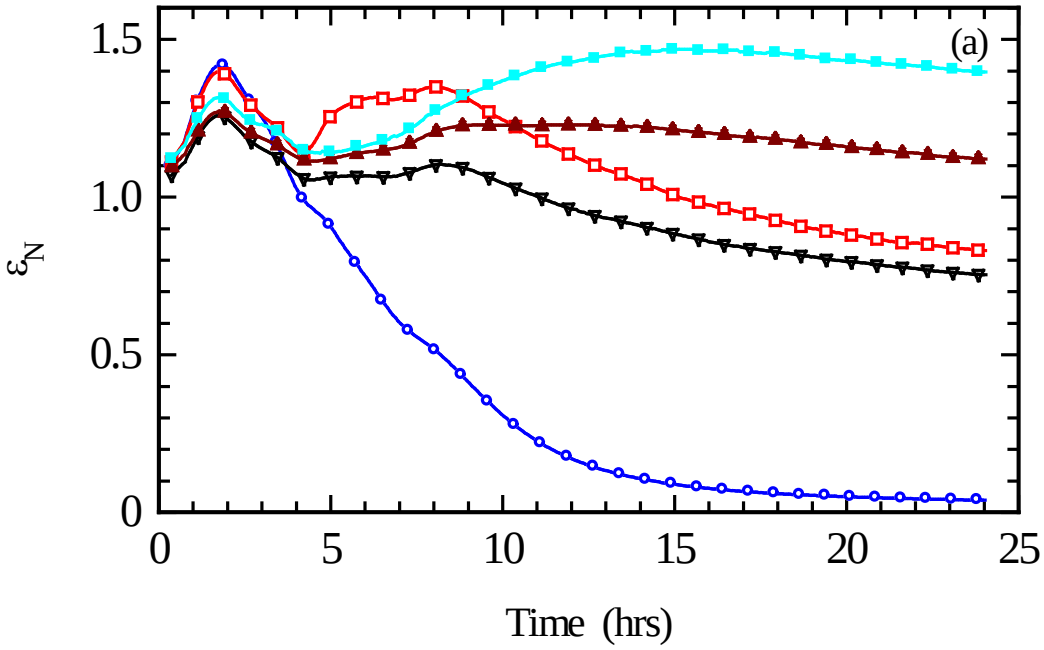
(a)
1.5
1.0
0.5
0
ε_N
0
5
10
15
20
25
Time (hrs)

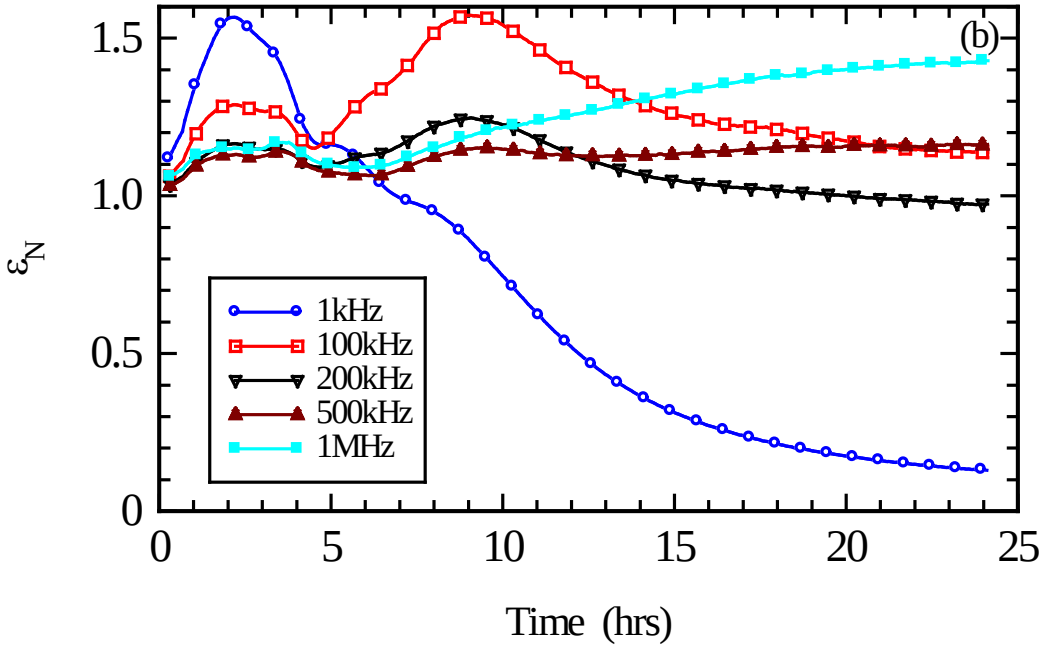
(b)
1.5
1.0
0.5
0
ε_N
1kHz
100kHz
200kHz
500kHz
1MHz
0
5
10
15
20
25
Time (hrs)

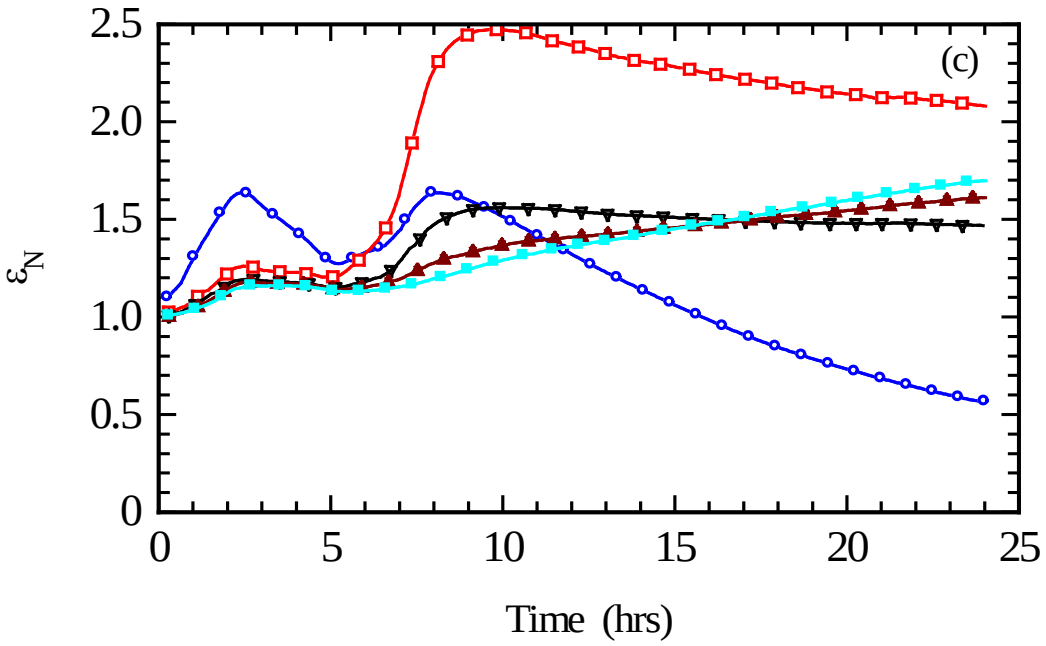

FIG. 9